Collective resonances in a circular array of gyromagnetic rods

Jin Wang [1,2] Kai Fung Lee,[2] Hui Yuan Dong,[3] Zheng-Gao Dong,[1] S. F. Yu,[2] and Kin Hung Fung [2,*]

[1]*School of Physics, Southeast University, Nanjing 211189, China*
[2]*Department of Applied Physics, Hong Kong Polytechnic University, Hong Kong, China*
[3]*School of Science, Nanjing University of Posts and Telecommunications, Nanjing 210003, China*

We present a rigorous theoretical investigation on the collective magnetic resonance of a circular array of subwavelength gyromagnetic rods. We derive the closed-form solutions to the eigenmodes within the framework of the dynamic dipole approximation using an eigenresponse theory. Owing to the lack of time-reversal symmetry and Lorentz reciprocity, the eigenpolarizability spectra exhibit significant nonreciprocal characteristics: only a single branch of rotating magnetic dipoles is supported, whereas another one corresponding to inversely rotating magnetic dipoles is totally suppressed. We found that the collective coupled magnetic dipole and coupled electric dipole (CED) modes of the circular arrays display remarkable distinction in both the resonant frequency and the radiative width in comparison with the isolated gyromagnetic rod. We further carry out full-wave numerical simulation to test the accuracy of the analytical results on the CED mode.

I. INTRODUCTION

Complex gyrotropic systems with many symmetries being broken and emergence of topological states have been studied intensively in recent years [1–12]. Owing to the broken time-reversal symmetry as well as broken Lorentz reciprocity, such gyrotropic systems can possibly exhibit unique nonreciprocal characteristics in the transmission of the field when the source and receiver are exchanged in their locations. For example, at the microwave frequency, magnetic photonic crystals based on gyromagnetic materials, i.e., yttrium iron garnet (YIG), were theoretically proposed [1] and experimentally verified [2,3] to realize the one-way electromagnetic edge mode, allowing light to propagate in one single direction but block light in the opposite direction. In the terahertz frequency regime, magnetized plasma or semiconductor materials, i.e., the indium antimonide (InSb), could be replaced to see the nonreciprocal phenomenon, i.e., one-way tunneling or one-way wave propagation [10]. Very recently, Pike and Stroud [11] investigated the propagation of spin waves on a periodic chain of spherical or cylindrical YIG particles induced by the magnetic dipole-dipole interaction and found that a linearly polarized wave will experience the Faraday rotation as it propagates along the particle chain, which is similar to the linear waves in bulk homogeneous magnetic materials.

Motivated by exploring electromagnetic properties in a gyrotropic system, in the present work we aim to see the collective optical response in a properly arranged circular array system composed of subwavelength gyromagnetic rods. Rather than just giving a simple physical picture, we show explicitly the analytical closed-form solutions to the intrinsic magnetic dipole (MD) mode for the proposed system within the framework of the dynamic dipole approximation. The

effective eigenpolarizability as well as the supporting mode patterns are described. It is indicated from the eigenpolarizability spectra of MD modes that only a single type of collective magnetic response is supported, arising from the specified rotating magnetic moment. Another type of the inversely rotating magnetic moment is completely suppressed. Such asymmetrical mode solutions originate from the nonreciprocal property of gyromagnetic materials. Moreover, the strong geometrical resonance of the array system yields a collective magnetic dipole (CMD) and coupled electric dipole (CED) mode, showing differences in both the resonant frequency and the radiative width in comparison with the resonance of an isolated gyromagnetic rod. As an example for validation, we further perform full-wave numerical simulations on the CED mode, showing good agreement with the analytical mode solutions.

The paper is organized as follows. In Sec. II, we describe the main geometry for the proposed array system and typical parameters used for gyromagnetic materials. By using the point MD model for each gyromagnetic rod, we derive in Sec. III the closed-form solutions to the magnetic eigenmodes based on the eigendecomposition method. Results on the eigenpolarizability spectra and the supported mode patterns are shown in Sec. IV. We further validate in Sec. V the analytical results on the CED mode by using full-wave numerical simulations and give the conclusions in Sec. VI. Throughout the paper, a monochromatic $e^{-i\omega t}$ time dependence is assumed.

II. GEOMETRY AND MATERIAL PARAMETERS

Let us consider N infinitely long cylindrical gyromagnetic rods with radius r arranged to have their centers located on a circle of radius R_0. A top view of the structure in the xy plane is schematically shown in Fig. 1(a), and the axis of each cylindrical rod is along the z direction. The center-to-center
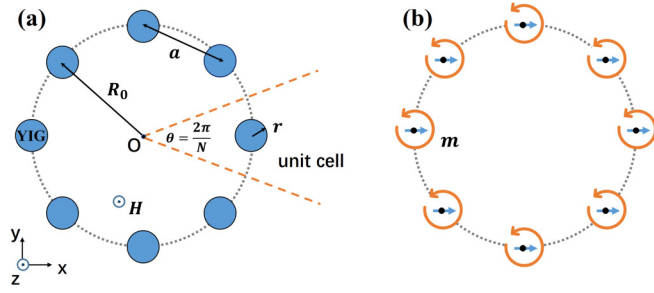
*kin-hung.fung@polyu.edu.hk

FIG. 1. (a) Schematic diagram of the circular array composed of N gyromagnetic (YIG) cylindrical rods. The geometrical parameters R_0, r, and a show the radius of the array structure, the radius of each individual rod, and the center-to-center distance between two nearest-neighbor rods, respectively. The unit cell for the array system is also presented. (b) The collection of N rotating MDs as an effective point dipole model of (a). The black dots denote the rod centers in (a), and the blue arrows show the excited magnetic moments $\mathbf{m}$ at the rods, the rotation directions of which are indicated by the orange circular arrows.

distance between two nearest-neighbor rods is identical with $a = 2R_0 \sin(\pi/N)$. The array is assumed to be centered at the origin and then the position vectors of the rod centers are described as

$$\mathbf{R}_j = R_0 \cos(2j\pi/N)e_x + R_0 \sin(2j\pi/N)e_y, \qquad (1)$$

where $j = 1, 2, \ldots, N$ is the rod index. Under the external static magnetic field H along the z direction, the gyromagnetic rod can be characterized by the permittivities ϵ_m and the following magnetic permeability tensor:

$$\boldsymbol{\mu} = \begin{pmatrix} \mu_1 & i\mu_2 & 0 \\ -i\mu_2 & \mu_1 & 0 \\ 0 & 0 & 1 \end{pmatrix}, \qquad (2)$$

where $\mu_1 = 1 + \omega_m(\omega_h - i\beta\omega)/[(\omega_h - i\beta\omega)^2 - \omega^2]$, $\mu_2 = \omega_m\omega/[(\omega_h - i\beta\omega)^2 - \omega^2]$, where $\omega_h = \gamma H_0$ is the precession frequency, γ is the gyromagnetic ratio, H_0 is the applied magnetic field, and β is the phenomenological damping coefficient; $\omega_m = \gamma 4\pi M_s$, and $4\pi M_s$ is the saturation magnetization. The background medium is set to be the vacuum. Notice that each individual rod may be treated as an ideal dipole in the limit of low-loss subwavelength structure near the frequency of its dipolar resonance. Meanwhile, we focus on the case that the rods are not too close together, i.e., $a \geqslant 3r$, retaining the validity of the dipole approximation for the entire array system. Hence in the following work, we may consider the proposed gyromagnetic system [shown in Fig. 1(a)] as a collection of N MDs in the xy plane, located respectively at the center of each rod [shown in Fig. 1(b)].

III. MODEL AND METHODS

A. Coupled dipole method

We start with a two-dimensional (2D) scattering problem of the collection composed of N MDs shown in Fig. 1(b), under the normal illumination of an external TE-polarized plane wave (H_x, H_y, E_z). The local field at the jth dipole consists of the external incident field acting on the jth dipole,

i.e., $\mathbf{H}^{\mathrm{inc}}(\mathbf{R}_j)$, and the field radiated from all other dipoles i ($i \neq j$). We then have the following equation for the field at the jth dipole,

$$\mathbf{H}^{\mathrm{loc}}(\mathbf{R}_j) = \mathbf{H}^{\mathrm{inc}}(\mathbf{R}_j) + \sum_{i \neq j}^{N} \mathbf{H}_i(\mathbf{R}_j - \mathbf{R}_i), \qquad (3)$$

where $\mathbf{H}_i(\mathbf{R}) = k_0^2 \mathbf{G}_0(\mathbf{R})\mathbf{m}_i$ is the magnetic field radiated from the magnetic moment $\mathbf{m}_i$ of the ith dipole. Here, $k_0 = \omega/c$ is the wave number in the background medium and $\mathbf{G}_0(\mathbf{R})$ is the free-space 2D Green's function.

The local field at the jth dipole induces a magnetic moment $\mathbf{m}_j = \boldsymbol{\alpha}\mathbf{H}^{\mathrm{loc}}(\mathbf{R}_j)$. Here, the polarizability $\boldsymbol{\alpha}$ is the dynamic dipole polarizability, which is represented by

$$\boldsymbol{\alpha} = \frac{8i}{k_0^2} \begin{bmatrix} (D_1 + D_{-1})/2 & -i(D_1 - D_{-1})/2 \\ i(D_1 - D_{-1})/2 & (D_1 + D_{-1})/2 \end{bmatrix}, \qquad (4)$$

where D_1/D_{-1} are the Mie scattering coefficients corresponding to the MD of the clockwise/counterclockwise rotating direction. It is emphasized that D_1 and D_{-1} are no longer the same for the gyromagnetic materials. The polarizability tensor in Eq. (4) indicates anisotropic characteristics with nonzero off-diagonal components, which substantially leads to the asymmetrical excitation on the MDs with different rotating direction. The derivation details for Eq. (4) and Mie scattering coefficients of an isolated gyromagnetic cylindrical rod are given in the Appendix.

To analyze the eigenmodes and mode profiles for this array of MDs, Eq. (3) may become

$$\boldsymbol{\alpha}^{-1}\mathbf{m}_j - k_0^2 \sum_{i \neq j}^{N} \mathbf{G}_0(\mathbf{R}_j - \mathbf{R}_i)\mathbf{m}_i = \mathbf{H}^{\mathrm{inc}}(\mathbf{R}_j), \qquad (5)$$

which are a set of linear equations for the coupled MDs. We may also write these equations in the compact matrix form

$$\mathbf{M}(\omega)\mathbf{m} = \mathbf{H}^{\mathrm{inc}}, \qquad (6)$$

where $\mathbf{m}$ is the $2N$-rowed column vector of N dipole moments ($\mathbf{m}_1, \mathbf{m}_2, \ldots, \mathbf{m}_N$) and $\mathbf{M}$ is a $2N \times 2N$ matrix, defined as

$$\mathbf{M}(\omega) = \boldsymbol{\alpha}^{-1} - k_0^2 \sum_{i \neq j}^{N} \mathbf{G}_0(\mathbf{R}_j - \mathbf{R}_i). \qquad (7)$$

Instead of solving Eq. (6) directly by a time-consuming method of searching complex zeros of the determinant of $\mathbf{M}$, $\det[\mathbf{M}(\omega)] = 0$, we consider the following eigenvalue problem:

$$\mathbf{M}(\omega)\mathbf{m} = \lambda(\omega)\mathbf{m}, \qquad (8)$$

by employing an eigendecomposition method (or spectral theory), which is previously known as an eigenresponse theory [13].

Here in Eq. (8), λ is the complex eigenvalue of the matrix $\mathbf{M}(\omega)$, and we can also define the effective eigenpolarizability as [14]

$$\alpha_{\mathrm{eig}} = \frac{1}{\lambda}, \qquad (9)$$

which allows us to see the collective response of the whole system when the external field is present. The imaginary part

of eigenpolarizability $\text{Im}[\alpha_{\text{eig}}]$ is proportional to the extinction of the external driving field. Its peaks also indicate the resonant mode location and the corresponding widths of the peaks are inversely proportional to the quality factor Q of the particular resonant mode. Moreover, the dominant contribution to the resonance from the material properties (material/site resonance) or the geometrical properties (geometrical/lattice resonance) can be generally separated.

B. Analytical eigensolutions

We now face the eigenvalue problem of Eq. (8) on the $2N \times 2N$ matrix $\mathbf{M}$, which in general is only solved numerically. Fortunately, the structure in Fig. 1(b) that we consider has a discrete rotational symmetry, and the above problem can be simplified and analytically solved as shown below.

For convenience, we present the matrix $\mathbf{M}$ and the magnetic dipole moments $\mathbf{m}$ in Eq. (8) using the Cartesian coordinates with an origin at the center of the circular array. Under a specified rotating transition by the matrix $\boldsymbol{\Omega}$,

$$\boldsymbol{\Omega} = \begin{bmatrix} \widetilde{\boldsymbol{\Omega}}_1 & \mathbf{O} & \mathbf{O} & \mathbf{O} & \mathbf{O} \\ \mathbf{O} & \widetilde{\boldsymbol{\Omega}}_2 & \mathbf{O} & \mathbf{O} & \mathbf{O} \\ \mathbf{O} & \mathbf{O} & \widetilde{\boldsymbol{\Omega}}_3 & \mathbf{O} & \mathbf{O} \\ \mathbf{O} & \mathbf{O} & \mathbf{O} & \ddots & \vdots \\ \mathbf{O} & \mathbf{O} & \mathbf{O} & \cdots & \widetilde{\boldsymbol{\Omega}}_N \end{bmatrix}, \quad (10)$$

where

$$\widetilde{\boldsymbol{\Omega}}_j = \begin{bmatrix} \cos(2j\pi/N) & \sin(2j\pi/N) \\ -\sin(2j\pi/N) & \cos(2j\pi/N) \end{bmatrix} (j = 1, 2, \ldots, N) \quad (11)$$

is the local transformation for the jth dipole, the eigenvalue problem Eq. (8) then becomes

$$\mathbf{M}'\mathbf{m}' = \lambda \mathbf{m}', \quad (12)$$

where the new vectors $\mathbf{m}' = \boldsymbol{\Omega}\mathbf{m}$ and new matrix $\mathbf{M}' = \boldsymbol{\Omega}\mathbf{M}\boldsymbol{\Omega}^{-1}$.

Due to the discrete rotation symmetry of the structure, it is seen that $\mathbf{M}'$ remains invariant under a cyclic index transformation, i.e., $\mathbf{T}(n)\mathbf{M}'\mathbf{T}(n)^{-1} = \mathbf{M}'$, for $n = 1, 2, 3, \ldots, N$, where

$$\mathbf{T}(n) = \begin{bmatrix} \mathbf{O} & \widetilde{\mathbf{I}} & \mathbf{O} & \mathbf{O} & \mathbf{O} \\ \mathbf{O} & \mathbf{O} & \widetilde{\mathbf{I}} & \ddots & \vdots \\ \mathbf{O} & \mathbf{O} & \mathbf{O} & \ddots & \mathbf{O} \\ \mathbf{O} & \mathbf{O} & \mathbf{O} & \ddots & \widetilde{\mathbf{I}} \\ \widetilde{\mathbf{I}} & \mathbf{O} & \mathbf{O} & \cdots & \mathbf{O} \end{bmatrix}^n, \quad (13)$$

and $\widetilde{\mathbf{I}}$ is a 2×2 identity matrix. Thereby, $\mathbf{T}(n)$ and $\mathbf{M}'$ may share the same eigenvectors

$$\mathbf{v}_n^{(p)} = \mathbf{g}^{(p)} e^{i2\pi pn/N}, \quad (14)$$

with $\mathbf{g}^{(p)}$ being an arbitrary vector and $p = 1, 2, 3, \ldots, N$.

By substituting Eq. (14) into Eq. (12) and introducing an additional index σ for further reduced eigenspaces, we can finally split the transformed Eq. (12), which is involved in the $2N \times 2N$ matrix $\mathbf{M}'$, into N sets of eigenvalue problems on a

2×2 matrix $\widetilde{\mathbf{M}}'^{(p)}$,

$$\widetilde{\mathbf{M}}'^{(p)}\mathbf{g}^{(p,\sigma)} = \lambda^{(p,\sigma)}\mathbf{g}^{(p,\sigma)}, \quad (15)$$

where

$$\widetilde{\mathbf{M}}'^{(p)} = \boldsymbol{\alpha}^{-1} - k_0^2 \mathcal{G}^{(p)}, \quad (16)$$

$$\mathcal{G}^{(p)} = \frac{i}{8} \sum_{j=1}^{N-1} \left[H_0^{(1)}(k_0 D_j)\widetilde{\boldsymbol{\Omega}}_j^{-1} + H_2^{(1)}(k_0 D_j)\mathbf{K} \right] e^{i2\pi pj/N}, \quad (17)$$

$$D_j = 2R_0 \sin\left(\frac{j\pi}{N}\right), \quad (18)$$

and

$$\mathbf{K} = \begin{bmatrix} -1 & 0 \\ 0 & 1 \end{bmatrix}, \quad (19)$$

with the mode index $p = 1, 2, 3, \ldots, N$, and $\sigma = +, -$.

The eigenvalues λ are given by

$$\lambda^{(p,\pm)} = \tfrac{1}{2}\left[\alpha_{11}^{-1} + \alpha_{22}^{-1} - \Sigma_2 \pm \Sigma_s\right], \quad (20)$$

with the corresponding eigenvectors

$$\mathbf{g}^{(p,\pm)} = \begin{bmatrix} a_{11}^{-1} - a_{22}^{-1} + \Sigma_3 \pm \Sigma_s \\ 2(\alpha_{21}^{-1} + \Sigma_1) \end{bmatrix}. \quad (21)$$

Note that the eigenvectors $\mathbf{m}'^{(p,\pm)}$ of $\mathbf{M}'$ are in the form of

$$\mathbf{m}_j'^{(p,\pm)} = \mathbf{g}^{(p,\pm)} e^{i2\pi pj/N}. \quad (22)$$

Here, some finite sums and expressions are used:

$$\Sigma_1 = \frac{ik_0^2}{8} \sum_{j=1}^{N-1} \sin\frac{2j\pi}{N} H_0^{(1)}(k_0 D_j) e^{i2\pi pj/N}, \quad (23)$$

$$\Sigma_2 = \frac{ik_0^2}{4} \sum_{j=1}^{N-1} \cos\frac{2j\pi}{N} H_0^{(1)}(k_0 D_j) e^{i2\pi pj/N}, \quad (24)$$

$$\Sigma_3 = \frac{ik_0^2}{4} \sum_{j=1}^{N-1} H_2^{(1)}(k_0 D_j) e^{i2\pi pj/N}, \quad (25)$$

and

$$\Sigma_s = \sqrt{4\left(\alpha_{12}^{-1} - \Sigma_1\right)\left(\alpha_{21}^{-1} + \Sigma_1\right) + \left(\alpha_{11}^{-1} - \alpha_{22}^{-1} + \Sigma_3\right)^2}. \quad (26)$$

Thus, the close-form solution to the eigenvalue problem for the circular array is eventually derived. It is seen from Eq. (21) that all eigenmodes are in general polarized elliptically in the xy plane with two possible types: clockwise ($\sigma = +$) or counterclockwise ($\sigma = -$) rotating MDs. As shown below, only one single type can actually be supported for the gyromagnetic system. Additionally, the phase difference between two nearest dipoles $\Delta j = 1$ on the mode index p is obtained with $2\pi p/N$ from Eq. (22).

IV. ANALYTICAL STUDY ON EIGENPOLARIZABILITIES AND FIELD PROFILES

We now analyze the nonreciprocal collective response in the proposed system through the eigenpolarizabilities and
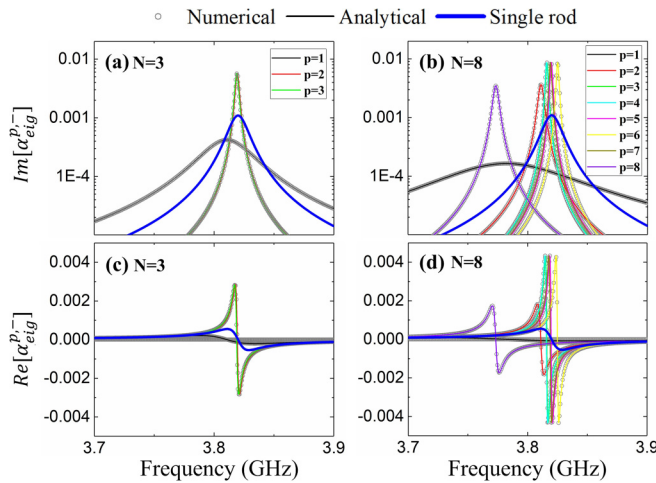
FIG. 2. Eigenpolarizability spectra for the rotating MD collections of $N = 3$ and $N = 8$. (a), (b) Imaginary part. (c), (d) Real part. The thin solid lines and the scatterers show the analytical results from Eq. (20) and numerical results by solving directly Eq. (8), respectively. For comparison, the eigenpolarizability spectra for the single isolated rod are also presented by solid blue lines. The eigenpolarizability is in arbitrary units.

the supporting field patterns. Without loss of generality, we consider here that the rods are made of a type of commercially available gyromagnetic material YIG, and use a set of typical parameters for YIG as $\epsilon_m = 15$, $H_0 = 500$ Oe, $4\pi M_s = 1750$ G, and $\beta = 3 \times 10^{-4}$. The geometrical parameters for the array system are set with $r = 0.08$ cm and $R_0 = 0.4$ cm. In Fig. 2, we calculate the real and imaginary parts of α_{eig} as functions of frequency using the analytical expression in Eq. (20). Cylindrical rods with different numbers for the array system are used, $N = 3$ in Figs. 2(a) and 2(c) and $N = 8$ in Figs. 2(b) and 2(d). The numerical data are also included in each figure by solving Eq. (8) directly with a commercial solver, i.e., Mathematica. Excellent agreement is shown between analytical and numerical results. In particular, for the array system composed of many rods, i.e., $N = 8$, analytical formulas allow us to trace the curves for different eigenmodes; otherwise it is difficult to connect the mixed numerical data points in Fig. 2 without analytical results.

For the imaginary part of each eigenpolarizability $\text{Im}(\alpha_{\text{eig}})$ as shown in Figs. 2(a) and 2(b), there always exists a typical Lorentzian peak, displaying the resonant frequency as well as the radiative width for the resonance, while for the real part $\text{Re}(\alpha_{\text{eig}})$, it changes from a peak to a dip close to the resonance. Owing to the violation of time-reversal symmetry and reciprocity, only a single branch ($\sigma = -$) of the counterclockwise rotating MDs is supported, whereas another one ($\sigma = +$) corresponding to the clockwise rotating MDs is completely suppressed with negligible eigenpolarizability. Meanwhile, all eigenmodes for $p = 1, 2, 3, \ldots, N$ are always nondegenerate, although some curves are in close proximity. Compared with the case of an isolated gyromagnetic rod (shown as blue lines in Fig. 2), the resonance for most of the collective modes mainly associated with material resonance

is close in frequency point to that for a single rod, i.e., modes $p = 2, 3$ in Fig. 2(a) or modes $p = 2, 3, \ldots, 7$ in Fig. 2(b). However, there are also additional mode solutions with a distinct redshift in the resonant frequency from that of single rod, resulting from the strong geometric resonance, i.e., mode $p = 1$ in Fig. 2(a) and $p = 1, 8$ in Fig. 2(b).

For the purpose of further understanding the complicated collective response, we plot in Figs. 3(a)–3(h) the electric field E_z patterns of all modes from $p = 1$ to $p = 8$ in the $N = 8$ array system, which is just the case of Figs. 2(b) and 2(d). For the $p = 1$ mode, magnetic moments in all MDs are rotating in a similar way, creating a CMD mode, while for the $p = 8$ mode, the excited magnetic moments form a circular loop of magnetic displacement current, representing effectively a CED mode. Other modes from $p = 2$ to $p = 7$ are involved in higher-order multipole moments, as shown in Figs. 2(b)–2(g). In terms of multipole decomposition, we can identify quantitatively the resonant character for each mode as shown in Figs. 3(i) and 3(j). The contributions of different multipoles (P_x, P_y, P_z, M_x, M_y, and M_z) are investigated by magnetic dipole moment $\mathbf{M} = \sum_j \mathbf{m}_j$ and electric dipole moment $\mathbf{P} = \frac{2}{ik_0} \sum_j \frac{\mathbf{R}_j \times \mathbf{m}_j}{R_j^2}$ [15,16]. For the $p = 1$ mode, large M_x and M_y components among these modes are seen, but with the $\pi/2$ phase difference between them, i.e., $M_y/M_x = e^{i\pi/2}$, resulting in the formation of a counterclockwise rotating MD in the xy plane. In comparison, a dominant scattering power attributed to the ED moment P_z is found for the $p = 8$ mode.

We next investigate in Fig. 4 the impact of MD numbers N on the mode distribution. Other geometrical parameters for the array system are fixed as those used in Fig. 2, i.e., $r = 0.08$ cm and $R_0 = 0.4$ cm. The position of each individual MD follows the formula Eq. (1). As N varies from $N = 2$ to $N = 10$, the interparticle distance becomes smaller and the interaction between MDs is enhanced, resulting in the formation of larger bandwidth (difference between maximum and minimum mode frequencies) as shown in Fig. 4. In particular, both the CMD ($p = 1$) and CED modes ($p = N$) are strongly influenced with an increase of N, indicating a much larger shift in the resonant frequency, whereas other modes are still near the resonance of a single rod (shown by the blue dashed line in Fig. 4).

Besides, the quality factor Q can also be evaluated from the imaginary part of eigenpolarizability $\text{Im}(\alpha_{\text{eig}})$, defined as $Q = \omega_0/\delta$ (the resonant frequency ω_0 and the corresponding peak width δ). In Fig. 5, we present the relative quantity Q/Q_0 for the CMD ($p = 1$) and CED ($p = N$) modes as a function of MD numbers N, showing the variation of the Q factor for the array structure compared to that (Q_0) for the single isolated rod. Notably, the CMD mode radiates strongly, resulting in the formation of a low-Q collective resonance. Meanwhile, the Q factor decreases gradually as N increases. In contrast, when the CED mode is excited, most of the electromagnetic energy tends to concentrate inside the array structure and the Q factor is well enhanced, particularly attaining a maximum $Q/Q_0 = 5.2$ for the case of $N = 3$. In addition, other higher-order collective modes except for the CMD and CED modes could also achieve an improvement of mode qualities (not shown).
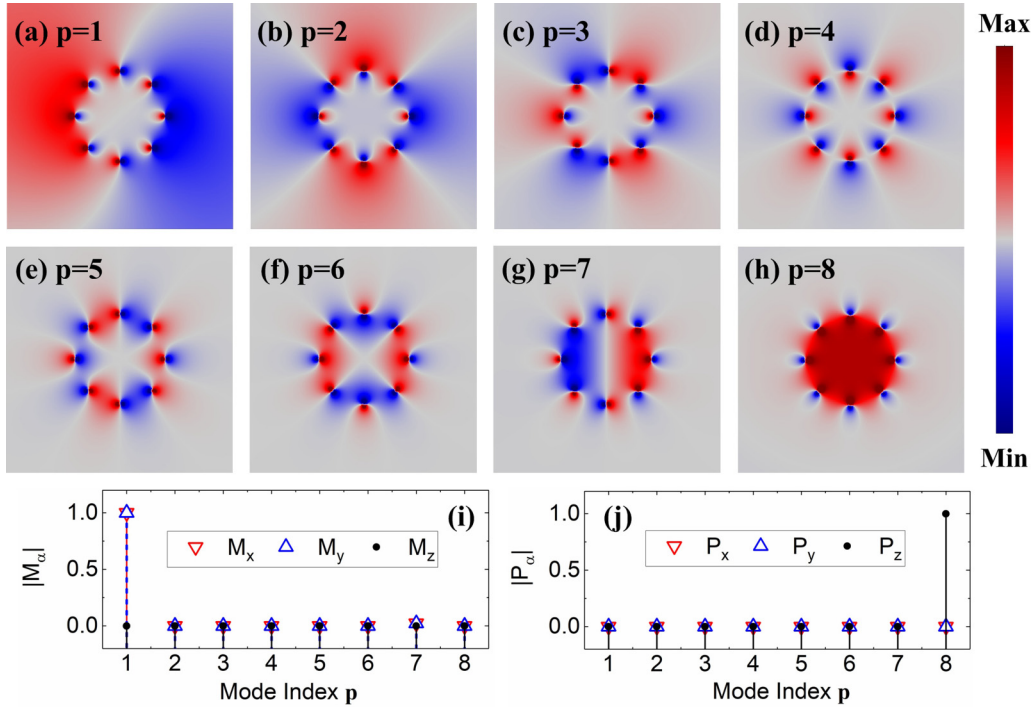
FIG. 3. (a)–(h) Electric field E_z patterns for the intrinsic normal modes of a ring of $N = 8$ counterclockwise rotating MDs. Normalized multipole decomposition results M_α (i) and P_α (j) of the normal modes to their respective maximal values in each panel.

V. VERIFICATIONS BY FULL WAVE NUMERICAL SIMULATION

We turn to carry out full-wave numerical simulations, i.e., COMSOL Multiphysics, to test the accuracy of the obtained analytical results within the framework of the dynamic dipole approximation used above. For our calculations, we choose a unit cell as shown in Fig. 1(a), due to the discrete rotational symmetry in the ring system. Two boundaries along the radial

directions are set by periodic conditions. For instance, the continuity in the fields of these two boundaries implies the case of an in-phase oscillation for all rods, also corresponding to that for the CED mode ($p = N$). The third boundary at the outer space is used by the scattering boundary. To see the eigenmode solutions, we then perform the mode analysis in COMSOL Multiphysics by probing a globe out-of-plane wave number k_z on the unit cell. Through sweeping the frequency over the concerned range, the magnitude of k_z may exhibit a dip close to zero when the resonance occurs. Field profiles can be used to further confirm which kind of resonance
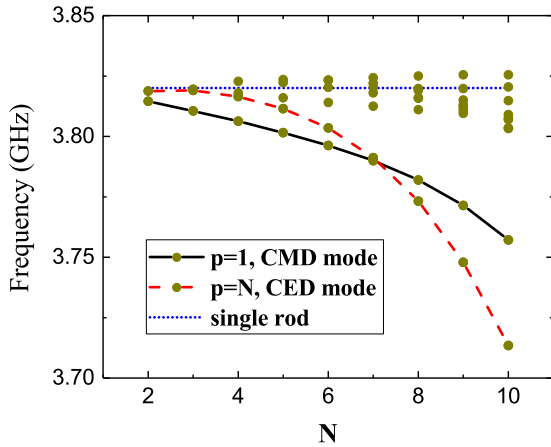

FIG. 4. The distributions of the resonant frequency as functions of the number N of the ring system. Analytical mode solutions on the CMD mode ($p = 1$) and CED mode ($p = N$) are also shown clearly by the black solid and red dashed lines, respectively. For comparison, the resonant frequency for the single isolated rod with radius $r = 0.08$ cm is indicated by the blue dotted line. The structural parameters R_0 and r are the same as those in Fig. 2.
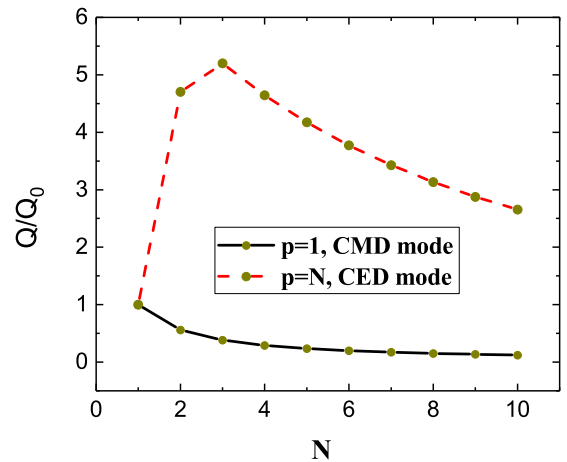

FIG. 5. The relative mode qualities Q/Q_0 of the CMD ($p = 1$) and CED ($p = N$) modes versus the number N of the ring system, where Q_0 is the Q factor for the single isolated rod with radius $r = 0.08$ cm. Other parameters are the same as those in Fig. 2.
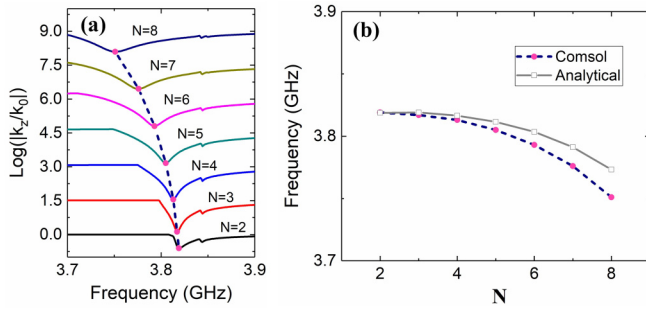
FIG. 6. (a) The globe out-of-plane wave number k_z on the chosen unit cell as a function of frequency. For different numbers N of ring systems, the CED modes are marked by pink dots and also connected with the dashed line. Note that each curve is shifted by 1.5 with respect to the preceding one. (b) The comparison of CED mode solutions between the COMSOL Multiphysics and analytical method. Other parameters are the same as those in Fig. 2.

happens, i.e., dipole, quadrupole, or other high-order multipole resonances.

In Fig. 6(a), we focus on the observation of the CED resonance by marking the lowest dips in magnitude of k_z for different ring systems analyzed in Fig. 4. A summary in the resonant frequency for the CED resonance is given in Fig. 6(b), showing good agreement with the analytical results. Nevertheless, discrepancies will exist for larger-N ring systems, mainly due to the neglected contribution of the ED resonance at the single isolated rod. As seen from Fig. 8 in the Appendix, the Mie coefficient D_0 (associated with the ED resonance) appears nearly unchanged, but just an order of magnitude less than that of D_{-1} (corresponding to the MD resonance) over the concerned frequency range; therefore the exclusion of D_0 may induce the noticeable shift in the resonant frequency.

We finally see in Fig. 7 the excitation of the CED resonance for the array system of $N = 3$ and $N = 8$ when an
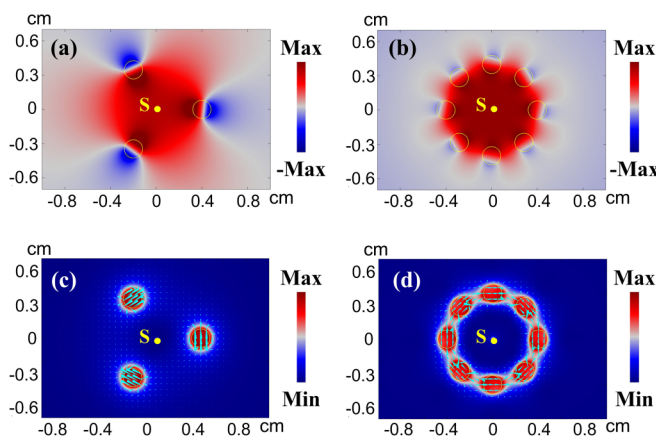

FIG. 7. The excitation of the CED resonance for the ring system of $N = 3$ and $N = 8$ when an out-of-plane electric current is located at the origin (labeled with S). (a), (b) The electric field profile E_z. (c), (d) Norm of magnetic field distribution $|H|$ simultaneously with the cyan arrows denoting the vector patterns of magnetic field $\mathbf{H} = (H_x, H_y)$. The structural parameters are $R_0 = 0.4$ cm and $r = 0.08$ cm.
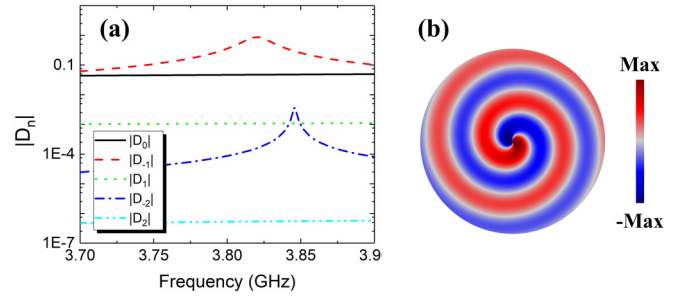

FIG. 8. (a) Magnitudes of the Mie scattering coefficients of a single isolated YIG cylindrical rod, having radius $r = 0.08$ cm, as depicted in Fig. 1(a). For TE polarization (H_x, H_y, E_z), the curve D_0 denotes the electric dipole, D_{-1}/D_1 the counterclockwise/clockwise rotating magnetic dipole, and D_{-2}/D_2 the counterclockwise/clockwise rotating magnetic quadrupole. The counterclockwise magnetic dipole is dominant over the range of frequencies, i.e., 3.7–3.9 GHz. (b) Radiation distribution maps on electric field (E_z component) for 2D counterclockwise rotating magnetic dipole, $m_y = im_x$, in free space.

out-of-plane electric current is located at the origin. The distributions in the electric field E_z [Figs. 7(a) and 7(b)] and the magnetic field $\mathbf{H} = (H_x, H_y)$ as well as norm of magnetic field $|H|$ [Figs. 7(c) and 7(d)] are shown in Fig. 7. At the resonance of dipolar MDs, i.e., $f = 3.817$ GHz for $N = 3$ or $f = 3.751$ GHz for $N = 8$, the rotating MD located at each individual rod is excited as shown by the cyan arrow surface of the magnetic field $\mathbf{H}$ in Figs. 7(c) and 7(d). Notice that there exists the abrupt change in direction of the magnetic field at the interface of the rod, due to the fact that the effective permeability $(\mu_1^2 - \mu_2^2)/\mu_1$ for each rod shows negative value at the dipolar MD resonance. Nevertheless, the in-phase oscillation patterns for all magnetic moments on rods form a circulation of magnetic displacement current, acting as an ED parallel to the rod axis. Thereby the excitation of the CED mode P_z is well observed. It is emphasized that the CED resonance is a collective response of the MDs among the rods, not possible with a single rod. Moreover, as the localized electric field mainly radiates inward, the CED resonance can be readily excited by a line current located at an arbitrary location inside the array system, not limited to the region close to the rod.

VI. CONCLUSION

In summary, we demonstrate an analytical approach to the coupled magnetic resonance in a circular array of subwavelength gyromagnetic rods. Based on the dynamic dipole approximation, we derive the closed-form formulas to the intrinsic MD mode solutions. Both the effective eigenmode polarizability and the supporting mode profiles are explicitly described. Owing to the unique property originating from gyromagnetic materials, i.e., the breaking of time-reversal symmetry and Lorentz reciprocity, significant nonreciprocal characteristics are exhibited: a class of MDs with the specified rotating direction is supported, whereas another one in inversely rotating MDs vanishes. In contrast to the resonance of an isolated gyromagnetic rod, the collective response for the array system, i.e., the collective CMD and CED resonance,

shows remarkable difference in the resonant frequency as well as the radiative width. The investigation on unique optical properties of subwavelength gyromagnetic structures may lead to potential applications in on-chip isolators, circulators, and nonreciprocal metasurfaces, which are expected to be key elements in modern communication.

APPENDIX: DYNAMIC POLARIZABILITY OF AN ISOLATED GYROMAGNETIC ROD

We consider a two-dimensional (2D) scattering problem of an isolated gyromagnetic rod with radius r under the normal illumination of an external TE-polarized plane wave (H_x, H_y, E_z). The material parameters and other geometrical settings are the same as those for the single rod depicted in Fig. 1(a). For convenience, we solve this problem by using a system of local cylindrical coordinates (ρ, ϕ) with an origin located at the center of the single rod. We expand the incident electric field by the cylindrical wave functions with $\mathbf{E}^{\mathrm{inc}}(\rho, \phi) = \sum_n A_n J_n(k_0 \rho) e^{in\phi} e_z$. Near the dipolar resonance of the subwavelength rod, one may treat it as a corresponding dipole. The magnetic field scattered by such a single rod is equivalent to that by a magnetic dipole $\mathbf{m}$, and thereby reads

$$\mathbf{H}^{\mathrm{sca}}(\rho, \phi) = k_0^2 \mathbf{G}_0(\rho)\mathbf{m} = k_0^2 \mathbf{G}_0(\rho)\boldsymbol{\alpha}\mathbf{H}^{\mathrm{inc}}(\rho, \phi), \quad \text{(A1)}$$

where $\boldsymbol{\alpha}$ denotes the dynamic polarizability tensor for the isolated gyromagnetic rod, and $\mathbf{G}_0(\rho)$ is the free-space 2D Green's function expressed by

$$\mathbf{G}_0(\rho) = \frac{i}{4}\begin{bmatrix} \frac{1}{x_f}H_1^{(1)}(x_f) & 0 \\ 0 & H_0^{(1)}(x_f) - \frac{1}{x_f}H_1^{(1)}(x_f) \end{bmatrix}, \quad \text{(A2)}$$

and

$$\mathbf{H}^{\mathrm{inc}}(\rho, \phi) = \sum_n \frac{k_0 A_n}{i\omega\mu_0}\begin{bmatrix} \frac{in}{x_f}J_n(x_f) \\ -J_n'(x_f) \end{bmatrix} e^{in\phi}, \quad \text{(A3)}$$

$$\mathbf{H}^{\mathrm{sca}}(\rho, \phi) = \sum_n \frac{k_0 B_n}{i\omega\mu_0}\begin{bmatrix} \frac{in}{x_f}H_n^{(1)}(x_f) \\ -H_n'^{(1)}(x_f) \end{bmatrix} e^{in\phi} \quad \text{(A4)}$$

are the incident and scattered magnetic fields, respectively. The Mie scattering coefficient $D_n (\equiv B_n/A_n)$ reads

$$D_n = \frac{x_f J_n(x_g)J_n'(x_f) - \zeta(x_g)J_n(x_f)}{x_f J_n(x_g)H_n'^{(1)}(x_f) - \zeta(x_g)H_n^{(1)}(x_f)}, \quad \text{(A5)}$$

with

$$\zeta(x_g) = n\mu_k J_n(x_g) + x_g \mu_r J_n'(x_g), \quad \text{(A6)}$$

where $J_n(x_f)$, $J_n(x_g)$, $H_n^{(1)}(x_f)$, $H_n^{(1)}(x_g)$, and the primes in Eqs. (A2)–(A6) respectively denote the nth-order Bessel and

the first kind of Hankel functions and their corresponding derivatives with the argument of $x_f = k_0 r$ (or $x_g = x_f\sqrt{\epsilon_m/\mu_r}$), $\mu_r = \mu_1/(\mu_1^2 - \mu_2^2)$, and $\mu_k = -\mu_2/(\mu_1^2 - \mu_2^2)$, and k_0 is the wave vector in free space.

Notice that here the incident wave we are concerned with should be the averaged local external magnetic field applied to the rod; thus the external incident wave at the center of the rod $H^{\mathrm{inc}}(\rho = 0)$ is only considered. However, most of the terms in Eq. (A3) at $\rho = 0$ can be proven to vanish, except the $n = \pm 1$ terms which reduce the field to

$$\mathbf{H}^{\mathrm{inc}}(\rho = 0) = \frac{k_0}{2\omega\mu_0}\left(\begin{bmatrix} 1 \\ i \end{bmatrix}e^{i\phi} + \begin{bmatrix} 1 \\ -i \end{bmatrix}e^{-i\phi}\right). \quad \text{(A7)}$$

Meanwhile, the main contribution of dipolar scattering field which comes from the $n = \pm 1$ items in Eq. (A4) combines Eq. (A1) and (A2), giving the effective magnetic dipole moment as follows:

$$\mathbf{m} = \frac{4i}{\omega k_0 \mu_0}\left(D_1\begin{bmatrix} 1 \\ i \end{bmatrix}e^{i\phi} + D_{-1}\begin{bmatrix} 1 \\ -i \end{bmatrix}e^{-i\phi}\right). \quad \text{(A8)}$$

Substituting Eqs. (A7) and (A8) into Eq. (A1), and matching the exponential term $e^{\pm i\phi}$, the relation between the dynamic polarizability tensor and Mie scattering coefficients yields

$$\boldsymbol{\alpha}\begin{bmatrix} 1 \\ \pm i \end{bmatrix} = \frac{8i}{k_0^2}D_{\pm 1}\begin{bmatrix} 1 \\ \pm i \end{bmatrix}, \quad \text{(A9)}$$

and the dynamic polarizability is finally written as

$$\boldsymbol{\alpha} = \frac{8i}{k_0^2}\begin{bmatrix} (D_1 + D_{-1})/2 & -i(D_1 - D_{-1})/2 \\ i(D_1 - D_{-1})/2 & (D_1 + D_{-1})/2 \end{bmatrix}. \quad \text{(A10)}$$

For a single gyromagnetic rod, the Mie scattering coefficients D_n and D_{-n} are no longer the same, due to the breaking of time-reversal symmetry arising from the presence of the external static magnetic field [seen from Eqs. (A5) and (A6)]. Let us look at a concrete example of a single YIG rod with radius $r = 0.08$ cm. The top view in the xy plane is similar to that in Fig. 1(a). The external static magnetic field is along the axis z of the rod. It is seen that the responses of the order n and $-n$ of magnetic dipole or quadrupole terms are different and not symmetric. Here, the scattering D_{-1} of the counterclockwise rotating magnetic dipole, with the moment $(m_y = im_x)$, is dominant over all other terms, including D_1 for the clockwise rotating dipole. Thereby, it is a good approximation for such a YIG rod to act as a specified rotating magnetic dipole, i.e., for the frequency range between 3.7 and 3.9 GHz. In Fig. 8(b), we further take a look at the radiation pattern of a 2D counterclockwise rotating magnetic dipole at the dipolar resonance, and plot the electric field (E_z component) distribution maps for its radiation in free space. It is found that a nonreciprocal spiral-like radiation pattern is formed, and the handedness associated with the rotating direction of MD will be flipped upon the magnetization reversal.

[1] F. D. M. Haldane and S. Raghu, Phys. Rev. Lett. **100**, 013904 (2008).

[2] Z. Wang, Y. Chong, J. D. Joannopoulos, and M. Soljačić, Nature (London) **461**, 772 (2009).

[3] Y. Poo, R.-X. Wu, Z. Lin, Y. Yang, and C. T. Chan, Phys. Rev. Lett. **106**, 093903 (2011).

[4] J. Wang, K. H. Fung, H. Y. Dong, and N. X. Fang, Phys. Rev. B **84**, 235122 (2011).

[5] A. Davoyan and N. Engheta, Nat. Commun. **5**, 5250 (2014).

[6] J. Wang, H. Y. Dong, C. W. Ling, C. T. Chan, and K. H. Fung, Phys. Rev. B **91**, 235410 (2015).

[7] C. W. Ling, J. Wang, and K. H. Fung, Phys. Rev. B **92**, 165430 (2015).

[8] S. Lin, S. Silva, J. Zhou, and D. Talbayev, Adv. Opt. Mater. **6**, 1800572 (2018).

[9] D. Floess and H. Giessen, Rep. Prog. Phys. **81**, 116401 (2018).

[10] Q. Y. Shi, H. Y. Dong, K. H. Fung, Z.-G. Dong, and J. Wang, Opt. Express **26**, 33613 (2018).

[11] N. A. Pike and D. Stroud, Eur. Phys. J. B **90**, 59 (2017).

[12] B. Fan, M. E. Nasir, L. H. Nicholls, A. V. Zayats, and V. A. Podolskiy, Adv. Opt. Mater. **7**, 1801420 (2019).

[13] K. H. Fung and C. T. Chan, Opt. Lett. **32**, 973 (2007).

[14] K. H. Fung, A. Kumar, and N. X. Fang, Phys. Rev. B **89**, 045408 (2014).

[15] T. Kaelberer, V. A. Fedotov, N. Papasimakis, D. P. Tsai, and N. I. Zheludev, Science **330**, 1510 (2010).

[16] L. Liu, L. Ge, P. Hu, H. Xiang, W. Yang, Q. Liu, and D. Han, J. Phys. D: Appl. Phys. **51**, 035106 (2018).